ChemPlusChem

Research Article
doi.org/10.1002/cplu.202200395

Chemistry Europe
European Chemical Societies Publishing

www.chempluschem.org

Tuning Magnetic and Photophysical Properties of Luminomagnetic Metal-Organic Framework Composites in an Inverse Core-Satellite Structure

Marcel T. Seuffert,[a] Tim Granath,[b] Thomas Kasper,[a] Ruben Maile,[a] Rosa Pujales-Paradela,[b] Johannes Prieschl,[b] Susanne Wintzheimer,[b, c] Karl Mandel,[b, c] and Klaus Müller-Buschbaum*[a, d]

Luminomagnetic composites have been synthesized that allow for an individual tuning of luminescence intensity, chromaticity and magnetization by combination of superparamagnetic, citrate-stabilized iron oxide nanoparticles with the luminescent MOFs $^{3}_{\infty}[Ln_2(BDC)_3(H_2O)_4]$ (Ln=Eu, Tb; BDC^{2-} = terephthalate). The components are arranged to a concept of inverse structuring compared to previous luminomagnetic composites with MOF@magnetic particle (shell@core) composition so that the luminescent MOF now acts as core and is covered by magnetic nanoparticles forming the satellite shell. Thereby, the magnetic and photophysical properties are individually tuneable between high emission intensity ($1.2 \cdot 10^6$ cps mg^{-1}) plus low saturation magnetization (6 emu g^{-1}) and the direct opposite ($0.09 \cdot 10^6$ cps mg^{-1}; 42 emu g^{-1}) by adjusting the particle coverage of the MOF. This is not achievable with a core-shell structure having a magnetic core and a dense MOF shell. The composition of the composites and the influence of different synthesis conditions on their properties were investigated by SEM/EDX, PXRD, magnetization measurements and photoluminescence spectroscopy.

Introduction

Multifunctional composites are compounds that enable a merging of inherent characteristics of multiple components into one system. This smart way of combining properties of multiple substances has gained growing interest in the recent years.[1,2,3,4] Metal-organic frameworks (MOFs) have become composite partners, whose combination with various materials is of increasing scientific interest. By arranging MOFs together with e.g., magnetic substances, it is possible to synthesize composite systems featuring magnetism in combination with characteristics arising from the MOF's intrinsic properties and structure. To obtain MOF containing composites, methods like embedding,[5,6] layer-by-layer growth,[7] encapsulation,[8,9] or mixing[10] have been developed.[11,12] Examples for magnetic composites implying MOFs are systems containing ZIF-8[13,14] or IRMOF-3,[6] which are catalytically active. Utilizing the MOFs MIL-100[15] or PCN-222,[1] composites were reported being able to remove Cr(VI) or U(VI) from waste water. Furthermore, composites containing MIL-88A enable the application as drug carriers for medical purposes[16] and NH_2-MIL-53(Al) and NU-1000 for MOF crystal orientation.[17] By utilizing metal-organic frameworks based on lanthanides, luminomagnetic composites were achieved and investigated, e.g. as luminescent sensors[18,19] for different MOFs and magnetic materials. E.g., when titania coated iron or iron oxide particles are combined with the white-light emitting MOF EuTb@IFP-1, a composite system is obtained, which is magnetic, white in appearance, and even white luminescent.[20] In luminomagnetic examples, the MOF was arranged as shell at the outside and the magnetic material as core at the inside, the properties of the MOFs being important for potential applications, while the combination with magnetic components results in options either to separate the composite after usage, or to directly guide the materials to desired locations.

An example for constituents imparting magnetic properties to composites, are metallic iron or iron oxide nano- and microparticles.[2,4,11,20] Small particles as composite component require a stabilization against aggregation and agglomeration, since a uniform dispersion of a solid in a liquid facilitate a behaviour of this heterogeneous materials close to being homogeneous.[21] A way to achieve stabilization of e.g., iron

[a] M. T. Seuffert, T. Kasper, R. Maile, Prof. Dr. K. Müller-Buschbaum
Institute of Inorganic and Analytical Chemistry
Justus Liebig University Giessen
Heinrich-Buff-Ring 17
35392 Giessen (Germany)
E-mail: kmbac@uni-giessen.de
[b] T. Granath, Dr. R. Pujales-Paradela, J. Prieschl, Dr. S. Wintzheimer, Prof. Dr. K. Mandel
Department of Chemistry and Pharmacy
Friedrich Alexander University Erlangen-Nürnberg
Egerlandstraße 1
91058 Erlangen (Germany)
[c] Dr. S. Wintzheimer, Prof. Dr. K. Mandel
Fraunhofer Institute for Silicate Research
Neunerplatz 2
97082 Würzburg (Germany)
[d] Prof. Dr. K. Müller-Buschbaum
Center for Materials Research
Heinrich-Buff-Ring 16
35392 Giessen (Germany)

Supporting information for this article is available on the WWW under https://doi.org/10.1002/cplu.202200395

oxide nanoparticles is a modification with alkyl phosphonates and phosphates,[22] block-copolymers,[23] or carboxylates, such as oleic acid, to bind to the surface of particles and to hinder aggregation sterically and/or electrostatically.[24] Another commonly used carboxylate stabilizer for iron oxide particles is citric acid, which is capable of binding to the particle surface by hydrogen bonds, or one or two of its carboxylate functionalities.[24,25,26] In addition, the remaining, non-bonding functional groups make the particles amenable of establishing chemical bonds to other substances.[25]

For optimizing the luminescence intensity of the overall composite materials, the electronic exchange between the magnetic material and the luminescent compound needs to be minimized because of light absorption and luminescence quenching abilities of iron oxide.[27] Typically this is achieved by coating the respective particles with inert oxides like silica[4,18,19,28] or titania[20] prior to the functionalization with luminescent MOFs. These mediator materials lower the magnetization of the magnetic particles, but, also enable a binding to the metal ions of a luminescent MOF to oxide surface defects, such as O–H groups.

Up to now, typically, composites containing magnetite particles and MOFs form core-shell structures with iron oxide functioning as core material covered by a MOF shell.[4,6,9,13,19,28,29] There are only a few non-luminomagnetic examples, where roles are interchanged and MOFs, namely MIL-101[10,30] or MOF-5,[31] NH_2-MIL-53(Al) and NU-1000[16] represent the core material covered by an iron oxide particle shell. An inversion of roles has been reported for a solid material with YO_4:Eu^{3+} cores surrounded by silica, functionalized with iron oxide nanoparticles[32] and for β-$NaY_{0.8}Eu_{0.2}F_4$@γ-Fe_2O_3 core-satellite particles.[33] Herein, we describe the synthesis, properties and tunability of properties of such inverse core-satellite composites for luminescent, lanthanide-based MOFs. This leads to core-satellite composites, in which magnetic citrate-stabilized iron oxide nanoparticles cover MOF crystallites of $^3_\infty[Ln_2(BDC)_3(H_2O)_4]$ (Ln=Eu, Tb) as satellite shell (see Scheme 1) leading to options for an individual tuning of luminescence and magnetism, which would not be achievable by the core-shell functionalization mode having magnetic particles as core material and luminescent MOF as outer shell.

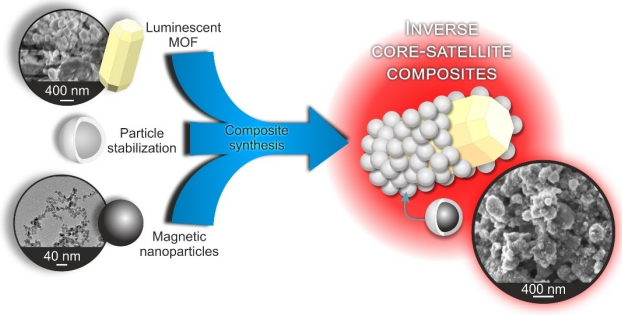

Scheme 1. Inverse core-satellite concept of composite systems comprising magnetic nanoparticles on top of a luminescent MOF, allowing also for a core-satellite arrangement

Results and Discussion

In this work, luminomagnetic composite systems were generated that achieve the goal to individually grant fine-tuning options for both, luminescence properties and magnetization. This has been accomplished by solvothermally combining superparamagnetic iron oxide nanoparticles (SPIONs) and the luminescent (MOFs) $^3_\infty[Eu_2(BDC)_3(H_2O)_4]$ (Eu–BDC) or $^3_\infty[Tb_2(BDC)_3(H_2O)_4]$ (Tb–BDC). SPIONs were chosen due to the high dispersibility and strong superparamagnetism and the respective MOFs because of their chemical and structural stability, as well as the intense luminescence.

The prepared composite systems do not build a core-shell structure with a MOF shell being deposited on the surface of the magnetic particles. The obtained composites instead exhibit an inverse core-satellite modification mode with inversion of roles of "core" and "shell", whereby MOF crystallites are covered to different extend by the magnetic satellite nanoparticles. Only this modification mode allows for the fine tunability of luminescence and magnetism.

In core-shell composites comprising a magnetic particle core and luminescent MOF shell, increasing the shell thickness leads to an increase in luminescence intensity while diminishing magnetization. From a certain layer thickness on, an increasing MOF amount would lower the magnetization further, while the luminescence intensity remains the same.

To the contrary, with an inverse core-shell modification mode, a dense magnetic shell would diminish the luminescence intensity. However, if the magnetic shell consists of nanoparticle satellites instead of a dense coating, the emitted light can propagate through the magnetic layer, resulting in the preservation of the photophysical properties of the luminescent MOF. Moreover, the luminescence intensity and the magnetization can be adjusted by varying the amount of magnetic particles covering the MOF. Additionally, since the magnetic particles function as outer shell, the dispersibility of the respective composites can be increased depending on the external functional groups of the particles.

To examine this tunability of properties of inverse core-satellite composites, differences in magnetization and luminescence properties were triggered and investigated in dependence of deliberate variation of the synthesis conditions. Thereby, the component ratio of iron oxide nanoparticles and MOF was adjusted to specific values, and the differences in photophysical and magnetic properties were examined in dependence of this ratio. Furthermore, the tunability of emission colour, and the stability of the inverse core-satellite composites against washing assisted by ultrasonication and synthesis in different solvents were examined.

Tunability of Emission Intensity and Saturation Magnetization of Inverse Core-Satellite Composites

To obtain luminomagnetic composites, the two solid components $^3_\infty[Ln_2(BDC)_3(H_2O)_4]$ (Ln–BDC, Ln=Eu, Tb) and superparamagnetic iron oxide nanoparticles (SPIONs, citrate-stabilized at

a pH of 2.1) were synthesized separately (see experimental section). The applied luminescent MOFs Ln–BDC contain trivalent lanthanide ions, which are eight-coordinate by oxygen atoms. Six of these oxygen atoms belong to carboxylate functions of terephthalate ligands, and two belong to coordinating water molecules (see Figure S1).[34] The identity and purity of the synthesized metal-organic framework was confirmed by powder X-Ray diffraction (PXRD, see Figure S2) and elemental analysis (see experimental section). The obtained crystallites of $^{3}_{\infty}[Eu_2(BDC)_3(H_2O)_4]$ are 255 nm (±170 nm) in size (hydrodynamic particle diameter), as shown by dynamic light scattering. The hydrodynamic diameter of crystallites of $^{3}_{\infty}[Tb_2(BDC)_3(H_2O)_4]$ were determined as 220 nm (±177 nm; see Figure S3). The magnetic nanoparticles consist of iron oxide in the magnetite structure, proven by PXRD (see Figure S4), and are approximately 10 nm in size according to transmission electron micrographs (see Figure S5), wherefore they are considered as nanoparticles. By dynamic light scattering a hydrodynamic particle diameter of 21 ± 10 nm was determined (see Figure S3). Considering the formation of a solvent shell, this corresponds with the results of TEM investigations. To prohibit agglomeration and aggregation, the nanoparticles were stabilized with citric acid. Hence, in the IR spectra of the stabilized particles, bands are present, which can be assigned to the functional groups of citric acid and Fe–O vibrations (see Figure S6).

To investigate the influence of the component ratio MOF:SPIONs on the properties of resulting composites, the amounts of MOF and SPIONs were adjusted to specific values. The resulting MOF:SPIONs weight ratio as well as the designation of the obtained composites are listed in Table 1. The composites are hereafter referred to as SPIONs@EuMOF-*x*, whereby *x* corresponds to the mass equivalents of MOF used for the synthesis. Powder diffraction patterns of the synthesized composites show reflections of both, $^{3}_{\infty}[Eu_2(BDC)_3(H_2O)_4]$ (which is isotypic to $^{3}_{\infty}[Tb_2(BDC)_3(H_2O)_4]$) and magnetite/maghemite (Fe_3O_4/γ-Fe_2O_3, the latter being a defective form of magnetite, which is hardly distinguishable for nanoparticles by PXRD) (see Figure 1). In the powder diffractograms, the intensity of the most intense reflection of $^{3}_{\infty}[Eu_2(BDC)_3(H_2O)_4]$ ($2\theta = 9.1°$) increases with a rising amount of MOF. Accordingly, the intensity of the most intense reflection of magnetite/maghemite ($2\theta = 35.5°$) is reduced with decreasing iron oxide content. Due to the low amount of SPIONs within the composites SPIONs@EuMOF-8 and SPIONs@EuMOF-10 (11 wt% and 9 wt%, respectively), this reflection has low intensity in the corresponding diffractograms. This proves, that both constituents are present within the obtained products and the used component weight ratios are directly associated with the ratio of luminescent and magnetic compounds within the composite.

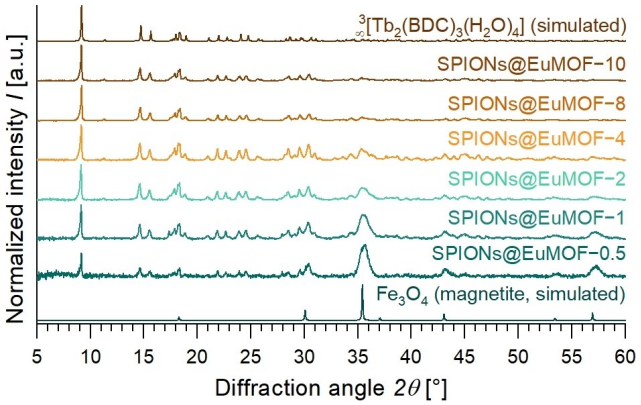

Figure 1. Powder X-ray diffractograms of synthesized composite systems SPIONs@EuMOF-*x* (containing SPIONs citrate-stabilized at pH 2.1) with different MOF:SPIONs weight ratios in comparison to the diffractograms of magnetite (Fe_3O_4)[37] and $^{3}_{\infty}[Tb_2(BDC)_3(H_2O)_4]$,[34] both simulated from respective single crystal diffraction data.

Electron micrographs of the synthesized composites show that they consist of crystallites, which are covered by smaller satellite particles, indicating the inverse core-satellite character. The coverage of crystallites by satellite particles gets more clear by comparison of electron micrographs of synthesized composites (e.g., SPIONs@EuMOF-2) and pure $^{3}_{\infty}[Eu_2(BDC)_3(H_2O)_4]$ (see Figure 2) equally treated to the synthesis procedure of the composites. The previously smooth surfaces of the MOF crystallites become coarse in appearance like the shape of "roasted almonds", when covered by iron oxide particles (see Figure 2). This morphology of the crystallite surfaces gradually increases with rising SPIONs amount (see Figure S7), being in good agreement with the inverse core-satellite functionalization mode with core-satellite character. This type of functionalization is further confirmed by transmission electron microscopy (TEM) of e.g., isolated SPIONs@EuMOF-4 composites (see Figure 3) indicating the combination of $^{3}_{\infty}[Eu_2(BDC)_3(H_2O)_4]$ and SPIONs on the nanometer scale. Thereby, the interaction of SPIONs with the MOF crystallite surfaces can be expected established

Table 1. Investigated weight ratio of MOF:SPIONs, amount of stabilized iron oxide nanoparticles in the product composites and composite designations.

Weight ratio MOF:SPIONs	Amount of iron oxide [wt%]	Composite designation
0.5:1	67	SPIONs@EuMOF-0.5
1:1	50	SPIONs@EuMOF-1
2:1	33	SPIONs@EuMOF-2
4:1	20	SPIONs@EuMOF-4
8:1	11	SPIONs@EuMOF-8
10:1	9	SPIONs@EuMOF-10

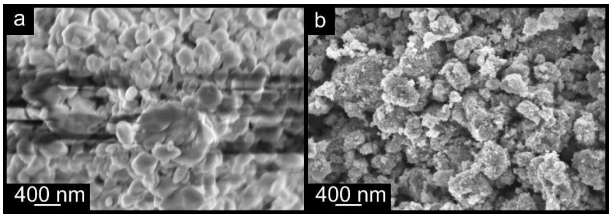

Figure 2. Scanning electron micrographs of a sample of pure $^{3}_{\infty}[Eu_2(BDC)_3(H_2O)_4]$ (Eu–BDC, a) in comparison to the composite SPIONs@EuMOF-2 (b).

Research Article
doi.org/10.1002/cplu.202200395
Chemistry Europe
European Chemical Societies Publishing

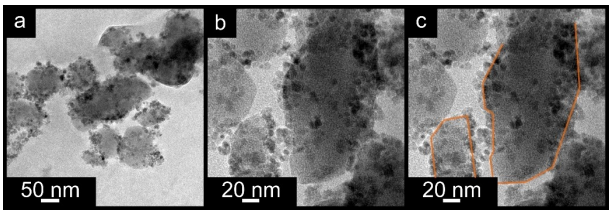

Figure 3. Transmission electron micrographs of isloated SPIONs@EuMOF-4 composites (a, b); a micrograph with surfaces of $^{3}_{\infty}[Eu_2(BDC)_3(H_2O)_4]$ highlighted, the surface coverage with SPION particles is imminent (c).

via C–O–Eu bonds between the citrate stabilization and the lanthanide ions.

The hydrodynamic particle size of the composites was determined and is, e.g., 390 ± 350 nm for SPIONs@EuMOF-4 (see Figure S8).

Energy dispersive X-ray spectra reveal that both, europium and iron are detectable near the surfaces of the coated crystals. Thereby, with decreasing amount of SPIONs, the signal strength and amount of detected aerial pixels, representing detected X-ray radiation characteristic for europium, increases, whereas, in case of iron, a drop in pixel density is observable (see Figure S9).

Besides these indications for co-localization of Eu–BDC and SPIONs, the presence of both constituents becomes evident by the magnetizability and, at the same time, homogeneous red-light emission upon UV excitation (see Figure 4) of the synthesized composites. The former arises from contained iron oxide nanoparticles. The latter appears due to the excitation of the photoluminescent compound $^{3}_{\infty}[Eu_2(BDC)_3(H_2O)_4]$ by irradiation with UV light.

The observed red emission is ion-specific for the lanthanide ion Eu^{3+}. This phenomenon upon UV irradiation is well known for lanthanide-containing coordination compounds and arises from a sensitizer effect of the ligand (in this case the BDC^{2-} ligand, which is responsible for light uptake). Energy transfer is finally followed by radiative decay[35,36] and red emission for the Eu^{3+} containing MOF.

Due to the described inverse core-satellite mode, the intensity of the light emission strongly depends on the selected MOF : SPIONs weight ratio with light emission intensity of the composite strongly increasing from SPIONs@EuMOF-0.5 (MOF : SPIONs = 0.5 : 1) to a MOF : SPIONs weight ratio of 10 : 1 (SPIONs@EuMOF-10, see Figure 4).

Excitation spectra of the synthesized substances (Figure 5) show a broad excitation band at 317 nm and red emission by intra-4*f*-transitions of Eu^{3+} in the emission spectra.[38] This complies with an energy transfer and antenna effect. Additionally, for pure Eu–BDC direct 4*f*–4*f* excitation bands are observable. They are hardly present for the composites, which can be explained by the absorbing nature of iron oxide[39] (see Figure S10). The emission spectra of synthesized compounds all show the characteristic emission bands for Eu^{3+} ions[38] (see Figure 5) resulting in red emission colour. Assignments of the observed transitions involved in the photoluminescence process are given in detail in Figure S11.

The chromaticity coordinates of SPIONs@EuMOF-*x* composites according to the *CIE* (Commission Internationale de l'Éclairage) *xy* colour space[40] are listed in Table S1. The

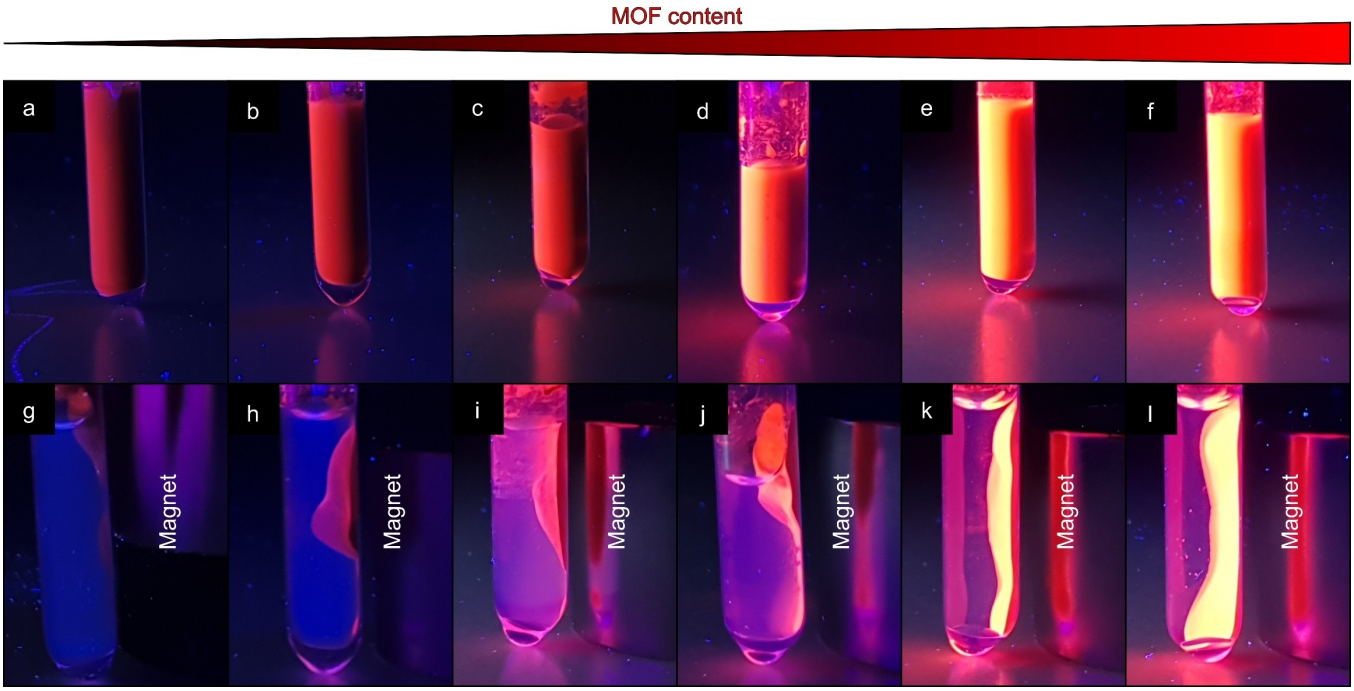

Figure 4. The synthesized composites SPIONs@EuMOF-*x* under UV excitation (λ_{exc} = 302 nm) without (a–f) and with (g–l) applying an external magnetic field for a growing MOF content for the MOF : SPIONs weight ratios listed in Table 1. a, g: SPIONs@EuMOF-0.5; b, h: SPIONs@EuMOF-1; c, i: SPIONs@EuMOF-2; d, j: SPIONs@EuMOF-4; e, k: SPIONs@EuMOF-8; f, l: SPIONs@EuMOF-10.

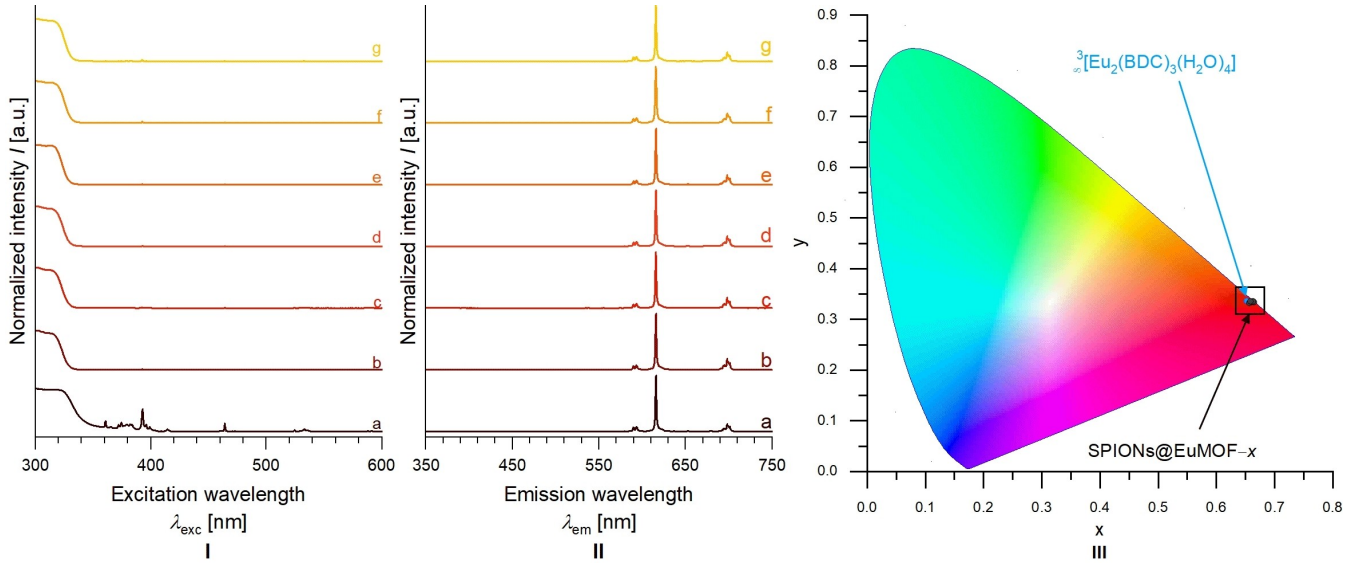

Figure 5. Normalized photoluminescence excitation (**I**) and emission spectra (**II**), as well as *CIE* chromaticity diagram with inserted chromaticity coordinates *xy* (**III**) of synthesized composites SPIONs@EuMOF-*x* in defined MOF : SPIONs weight ratios (see Table 1 and Table S1). a: pure MOF $^3_\infty[Eu_2(BDC)_3(H_2O)_4]$; b: SPIONs@EuMOF-0.5; c: SPIONs@EuMOF-1; d: SPIONs@EuMOF-2; e: SPIONs@EuMOF-4; f: SPIONs@EuMOF-8; g: SPIONs@EuMOF-10. Emission spectra were recorded at $\lambda_{exc} = 317$ nm. Excitation spectra were recorded for $\lambda_{em} = 616$ nm. Assingments of the transitions observed are given in Figure S11.

determined chromaticity for all is in good accordance to the chromaticity determined for pure Eu–BDC.

To quantify the observed gradual change in luminescence intensity, the mass-related emission intensity I_M of the synthesized substances was determined. Recorded emission intensities are listed in Table S2. The change in the luminescence intensity in dependence of the SPIONs content is not only influenced by a simple "dilution" of the luminescent compound with non-luminescent nanoparticles. The absorbing nature of iron oxide at both, the excitation and emission wavelengths of the luminescent MOF, also affects the emission intensity. Considering all these mechanisms the mass-related intensities I_M of the most intense emission band (at $\lambda_{exc} = 317$ nm) can be described according to

$$I_M = I_{max} \cdot (1 - p(\text{SPIONs})) \cdot \left(A_1 \cdot 10^{-A_1 \cdot p(\text{SPIONs})} + A_2 \cdot 10^{-\frac{A_2}{\Phi} \cdot p(\text{SPIONs})}\right) \cdot \frac{1}{\sum_{i=1}^{2} A_i} \quad (1)$$

with I_{max} as mass-related emission intensity I_M of pure Eu–BDC ($3.6(2) \cdot 10^6$ cps·mg^{-1}), p(SPIONs) as applied weight percentage of SPIONs (citrate-stabilized at pH = 2.1), A_1 as absorbance A of the iron oxide nanoparticles at $\lambda = 616$ nm (0.912) and A_2 as absorbance A at $\lambda = 317$ nm (1.779), and Φ as quantum yield of pure Eu–BDC ($\Phi = 0.126(2)$ for $\lambda_{exc} = 317$ nm, $\lambda_{em} = 550$–725 nm). The first, linear term of Equation 1 $I_M \cdot (1 - p(\text{SPIONs}))$ can be assigned to a "dilution" of a luminescent substance with a non-luminescent compound. This term is multiplied with a correction factor concerning the absorbance A of the non-luminescent compound at both, the emission (A_1) and the excitation wavelength (A_2). In addition to the absorbance, the quantum yield Φ influences the mass-related emission intensity and is added as a quotient in the exponent of the latter correction factor. Furthermore, the two absorption corrections are weighted with the respective absorbances A_1 and A_2, enforcing a normalization by $\Sigma A = A_1 + A_2$. The recorded mass-related emission intensities, a simulated curve of Equation 1, and a fit of Equation 1 to the recorded data is shown in Figure 6.

While fitting I_M, the quantum yield Φ of pure MOF was held constant at 0.126, while the other parameters (I_{max}, A_1, A_2) were refined freely. An adjusted coefficient of determination (COD) of 0.984 was reached, which confirms the accuracy of Equation 1 already apparent in Figure 6. The refined besides the determined parameters are listed in Table 2.

The quantum yields of the synthesized compounds decrease gradually with reducing the MOF content, as well. The decrease can thereby be described with an exponential decay function. However, due to the already described intensity influencing mechanisms, the quantum yield of the pure MOF exceeds the value expected according to the fit function, as it does not encompass the additional absorber (see Figure S12). For the pure MOF a quantum yield of 0.13(2) is reached, which is in good accordance to the published value of 0.14.[41] According to the exponential trend, the quantum yield for the pure MOF should reach a value of approximately 0.09(2).

Table 2. Determined and refined parameters of Equation 1. A simulated curve and fitted curve, as well as recorded mass related intensities I_M of the synthesized substances are depicted in Figure 6.

Parameter	Determined	Refined
I_{max} [10^6 cps·mg^{-1}]	3.6(2)	3.6(4)
A_1	0.91	1.3(2)
A_2	1.80	1.7(3)

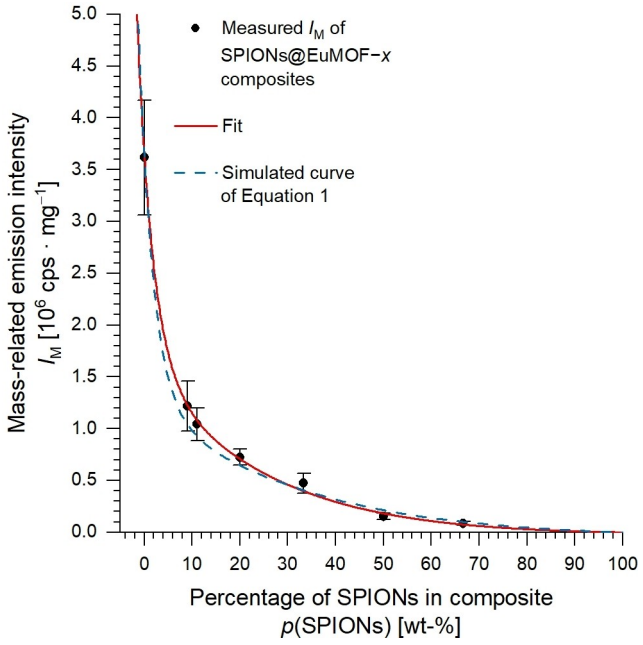

Figure 6. Determined mass-related emission intensities I_M (λ_{em} = 616 nm, λ_{exc} = 317 nm) of the composites SPIONs@EuMOF-x in dependence of the amount of SPIONs p(SPIONs) used for the synthesis of the composites (see Table S2), as well as a fit of Equation 1 besides a simulated curve of Equation 1. All variables except for the quantum yield Φ of the pure MOF were refined during the fit. Depicted error bars correspond to 3σ. The refined parameters are listed in Table 2. The adjusted coefficient of determination (COD) was 0.984.

In addition, the luminescence lifetime of the synthesized compounds was also investigated. The luminescence intensity decay of a sample of pure $^3{}_\infty$[$Eu_2(BDC)_3(H_2O)_4$] (Eu–BDC) treated analogously to the synthesis procedure of the composites (mortaring and solvothermal treatment, without addition of iron oxide nanoparticles) can be described with a monoexponential decay. The luminescence lifetime was determined as 0.4380(3) ms. For all composites comprising of Eu–BDC and iron oxide nanoparticles, the determined luminescence lifetimes are in the same range of approximately 0.4 ms (see Table S3). All these determined luminescence lifetimes match well the published value for $^3{}_\infty$[$Eu_2(BDC)_3(H_2O)_4$] of 0.40(4) ms.[41] Therefore, neither the solvothermal treatment in water, nor the presence of iron oxide nanoparticles on the crystallite surfaces of the luminescent lanthanide MOF influences the luminescence mechanism of the MOF other than light absorption. As a result, the electronic systems of the iron oxide nanoparticle part of the composites and of the MOF part do not interact.

Direct influence of the selected component ratio is also observed for the magnetization of the composites (see Figure 7). All composites show superparamagnetic behaviour, since no hysteresis is observed for the magnetization. This indicates the presence of magnetic *nanoparticles* as individual magnetic domains within the composites. The mass-related saturation magnetization M_S thereby increases for rising nanoparticle content and accordingly for decreasing MOF content.

Indeed, the saturation magnetization in dependence of the applied wt% of SPIONs and can be well described by a linear function. This indicates that the MOF:SPIONs ratios selected for syntheses match with the ratios in the respective products. The

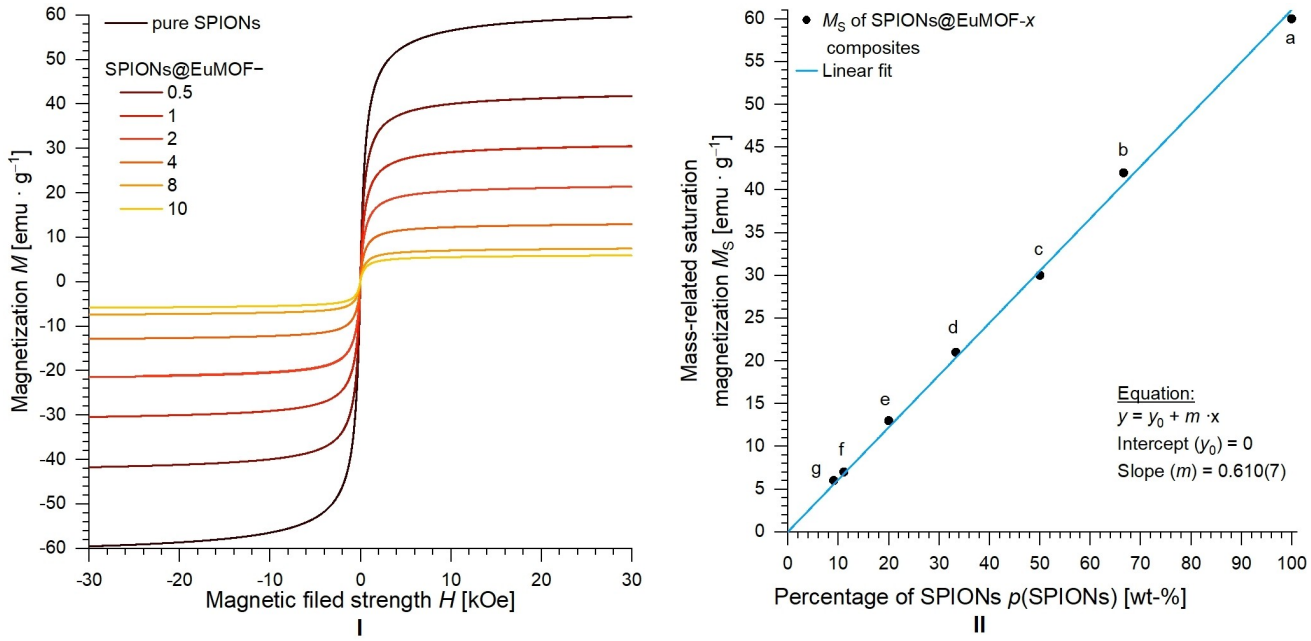

Figure 7. Magnetization curves of the composites SPIONs@EuMOF-x comprising $^3{}_\infty$[$Eu_2(BDC)_3(H_2O)_4$] and SPIONs, (citrate stabilized at pH = 2.1); with different MOF:SPIONs weight ratios (**I**) and mass-related saturation magnetizations M_S (see Table S2) of these composites in dependence of selected weight percentages p(SPIONs) of iron oxide nanoparticles (**II**). a: pure citrate-stabilized (pH = 2.1) iron oxide nanoparticles (p(NP) = 100 wt%); b: SPIONs@EuMOF-0.5 (p(NP) = 66.67 wt%); c: SPIONs@EuMOF-1 (p(NP) = 50.00 wt%); d: SPIONs@EuMOF-2 (p(NP) = 33.33 wt%); e: SPIONs@EuMOF-4 (p(NP) = 20.00 wt%); f: SPIONs@EuMOF-8 (p(NP) = 11.11 wt%); g: SPIONs@EuMOF-10 (p(NP) = 9.09 wt%).

linear approximation with an adjusted coefficient of determination of 0.999 shows, how accurate and precise the magnetization can be adjusted by choosing a defined component ratio. Therefore, the selected MOF:SPIONs ratio corresponds very well to the mass ratio of the two components in the product. Determined saturation magnetizations are listed in Table S2.

The presence of both components within the composites is further substantiated by the recorded IR spectra of the composites SPIONs@Eu–BDC, which show characteristic bands of the ligands (terephthalate and water) of the MOF,[34] as well as of citrate and iron oxide (see Figure S13). Additionally, the composition comprising Eu–BDC and SPIONs gets evident in the absorption spectra as well. Pure iron oxide particles absorb light in the entire visible range with rising absorbance for decreasing wavelength. The absorption spectrum of pure Eu–BDC MOF contains several narrow peaks low in intensity, which are assigned to 4*f*–4*f* transitions, and a broad, intense absorption band at approximately 310 nm, which can be assigned to the light absorption of the ligand within the MOF (see Figure S10 and Figure S11). These characteristics of both compounds are also present in the absorption spectra of the composites SPIONs@EuBDC, in which the absorption band at 310 nm becomes more dominant with increasing MOF content (see Figure S10).

Altogether, the combination of the performed analyses clearly indicates the tunability of both, saturation magnetization and emission intensity of the composite materials. An analogously deliberate tunability of properties would not be achievable with a core-shell structuring of a magnetic core and a MOF shell. In such a composite, the luminescence intensity would just increase with increasing MOF content to a saturation value, from which on additional MOF content would only lower the magnetization of the composites further and no significant influence on luminescence intensity would be further observable.

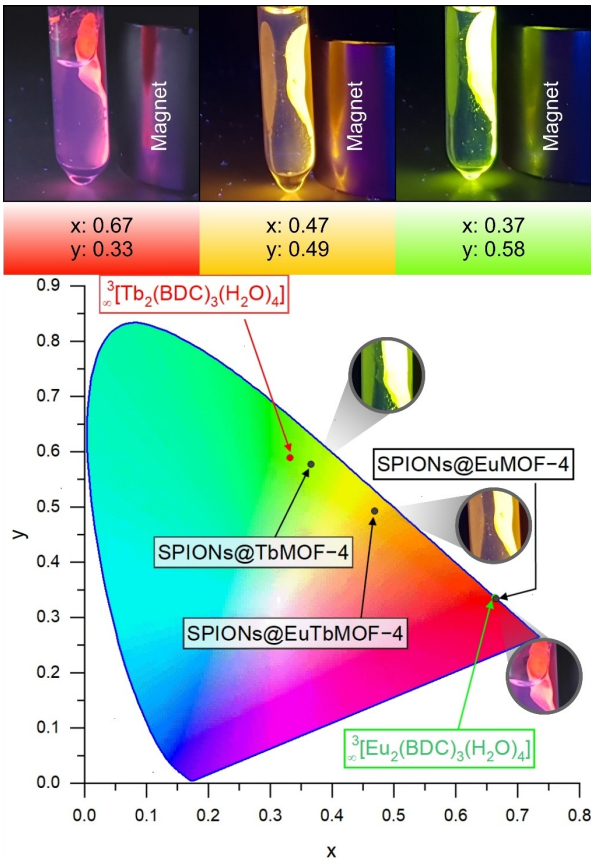

Figure 8. Composites SPIONs@EuMOF-4 (top left), SPIONs@EuTbMOF-4 (top center), and SPIONs@TbMOF-4 (top right), as well as corresponding *CIE* chromaticity coordinates *xy* (see Table S1) and a *CIE* chromaticity diagram with *xy* inserted as points (bottom). All composites contain SPIONs citrate-stabilized at pH = 2.1 (MOF(s):SPIONs weight ratio 4:1).

Tunability of Emission Chromaticity of the Inverse Core-Satellite Composites

Since the MOF $^3_\infty$[Eu$_2$(BDC)$_3$(H$_2$O)$_4$] is isotypic to the respective terbium-containing structure, the possibility of a composite containing other lanthanide containing MOFs of the constitution $^3_\infty$[Ln$_2$(BDC)$_3$(H$_2$O)$_4$], such as $^3_\infty$[Tb$_2$(BDC)$_3$(H$_2$O)$_4$] (Tb–BDC) or a combination of MOFs, can be utilized to tune the chromaticity of light emission in addition to the intensity. Hence, a synthesis analogous to the preparation of SPIONs@Eu-MOF-4 with a MOF:SPIONs weight ratio of 4:1 and SPIONs citrate-stabilized at pH = 2.1 was performed using Tb–BDC, as well as a 1:1 weight mixture of Tb–BDC and Eu–BDC. The obtained composite systems again exhibit magnetizability and intense luminescence (see Figure 8).

The composition and structuring of the composites were again investigated and confirmed by PXRD (see Figure S14), SEM/EDX (see Figure S15), and TEM (see Figure S16). These prove the simultaneous presence of crystallites of the MOF(s) and iron oxide particles deposited on their surfaces building the inverse core-satellite structuring with core-satellite character, and a homogeneous distribution of Tb, Eu and Fe analogously to the already described systems. The photoluminescence spectra of the composite containing both lanthanide MOFs (SPIONs@EuTbMOF-4) show the characteristic transitions of both lanthanide ions,[38,42] Eu^{3+} and Tb^{3+}, while the spectra of SPIONs@TbMOF-4 show characteristic bands of Tb^{3+} only (see Figure S17 and Figure S11). Accordingly, the colour of the light emission can be tuned by the selection of the ratio of Eu and Tb. In case of Tb containing composites, light absorption of the SPIONs needs to be considered when quantitatively evaluating the chromaticity because of the absorbance of SPIONs being increased in the green region of the visible spectrum.

Therefore, the emitted light of SPIONs@EuTbMOF-4 has a yellow colour, which arises from the mixture of the red emission of Eu^{3+} and the green emission of Tb^{3+} (see Figure 6). The determined chromaticity coordinates of the synthesized composites are listed in Table S1. The particle diameter according to dynamic light scattering of SPIONs@TbMOF-4 was determined to 115 ± 55 nm (see Figure S7).

The chromaticity of the composite SPIONs@TbMOF-4 differs from the pure MOF. While the *CIE* coordinates *xy* of pure Tb–BDC are located in the green region of the respective colour

space, the chromaticity coordinates of the composite containing both, iron oxide nanoparticles and Tb–BDC, are shifted towards red in comparison to pure Tb–BDC resulting in a yellowish-green emission colour (see Figure S18). This can be explained by light absorption by the iron oxide nanoparticles in the visible range (see Figure S10). Since the absorbance at low wavelengths is higher compared to the absorbance at high wavelengths, blue and green light is absorbed to a greater extend compared to red light. Therefore, the chromaticity of a composite containing Tb–BDC is shifted towards red in comparison to pure Tb–BDC. The emission spectra can be corrected by

$$I_0(\lambda) = I(\lambda) \cdot 10^{A(\lambda)} \quad (2)$$

with $I(\lambda)$ being the recorded emission intensity I at a certain wavelength λ, $A(\lambda)$ as the corresponding absorbance A of SPIONs at λ, and $I_0(\lambda)$ being the resulting corrected emission intensity at λ. The maximum absorbance of iron oxide nanoparticles was thereby normalized to 1. Subsequently – since the qualitative luminescence spectra were normalized to the most intense emission band ($\lambda = 545$ nm for SPIONs@TbMOF-4) – the normalized absorbance was adjusted to be 0 at the respective wavelength. Applying this correction, the spectral differences between SPIONs@TbMOF-4 and pure Tb–BDC diminish and the chromaticity coordinates converge (see Figure 9). Since the absorbance of iron oxide is low in the red region of visible spectrum (see Figure S10), the chromaticity of SPIONs@EuMOF-*x* composites does not require adjustment but already matches with the chromaticity of pure Eu–BDC and remains almost unaffected by the correction (see Figure S18).

A comparison of all determined chromaticity coordinates with and without applied absorption correction is listed in Table S4. This confirms the assumption the involved luminescence processes are not mechanistically affected by the presence of iron oxide nanoparticles except by light absorption.

Stability of the Inverse Core-Satellite Composites

To determine their stability, the synthesized SPIONs@EuMOF-4 composites were synthesised in different solvents (water, EtOH and cyclohexane) and washed several times (see experimental section). A change in ratio of constituents due to washing would be directly observable in magnetization of resulting substances. When comparing the magnetizations of SPIONs@EuMOF-4, without washing and after washing three, five, and eight times, no significant difference is observable, which proves the remarkable stability of inverse core-satellite composites and the inherent contact of the two components (see Figure 10).

Besides water, analogous syntheses of SPIONs@EuMOF-4 were performed in ethanol and cyclohexane to investigate the influence of different solvent polarities and hence dispersibility of iron oxide nanoparticles. Again, inverse core-satellite composites with a core-satellite character were obtained (see Figure S19), which consist of iron oxide nanoparticles and the MOF $^3_\infty[Eu_2(BDC)_3(H_2O)_4]$ (see Figure S20). The composite materials again exhibit strong magnetism and intense luminescence (see Figure 11). No significant differences, neither in SEM/EDX (see Figure S19), PXRD (see Figure S20), nor in magnetization investigations (see Figure S21) can be observed. Additionally, only minor influences on photoluminescent properties (see

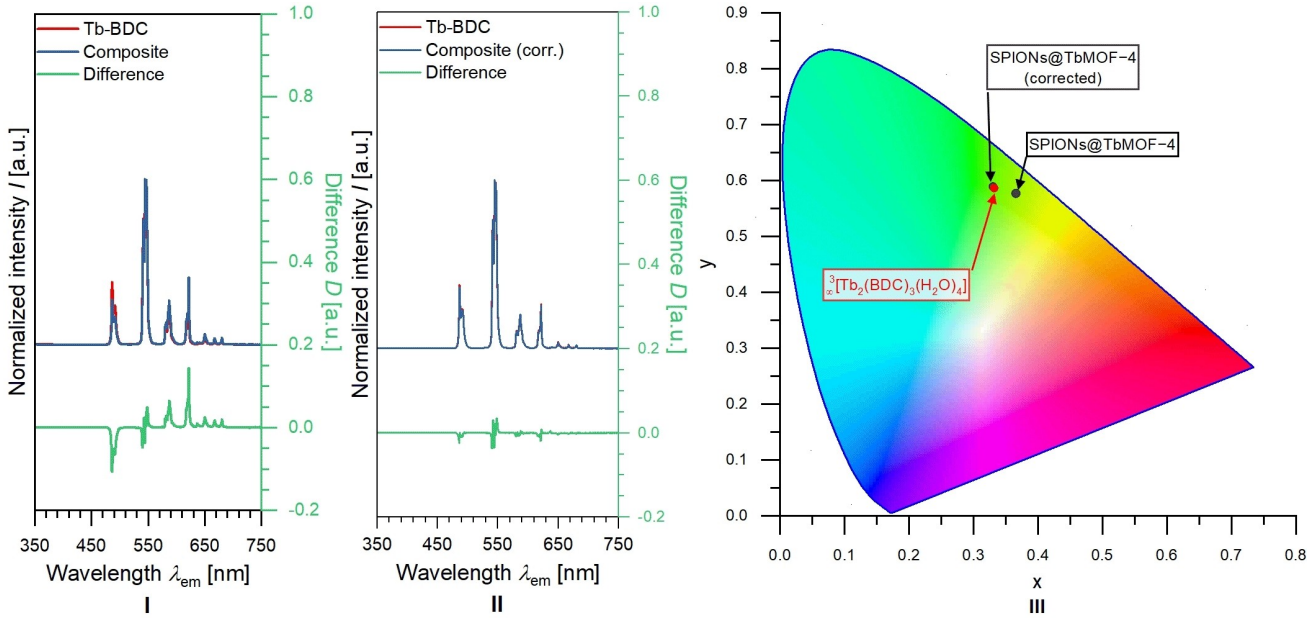

Figure 9. Emission spectra of TbMOF-4@NP (blue) and pure $^3_\infty[Tb_2(BDC)_3(H_2O)_4]$ (Tb–BDC, red) and the intensity difference of those (green) (**I**); Emission spectrum of TbMOF-4@NP (blue) corrected for the absorption of iron oxide nanoparticles (see Figure S6), emission spectrum of pure Tb–BDC (red) and the difference of those (green) (**II**); Chromaticity diagram according to *CIE* of TbMOF-4@NP (corrected for the absorption of iron oxide and as recorded) and of pure Tb–BDC (**III**). The intensity difference was calculated using I(TbMOF-4@NP) − I(Tb–BDC).

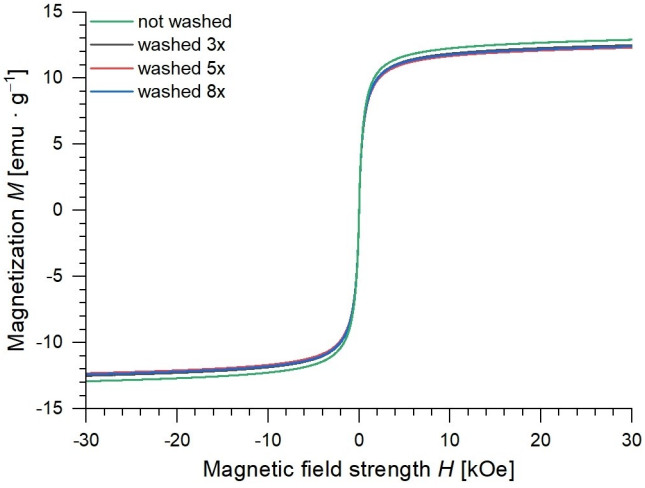

Figure 10. Magnetization of washed SPIONs@EuMOF-4 composites in comparison to the magnetization of as-synthesised SPIONs@EuMOF-4. The magnetization is almost identical for all samples.

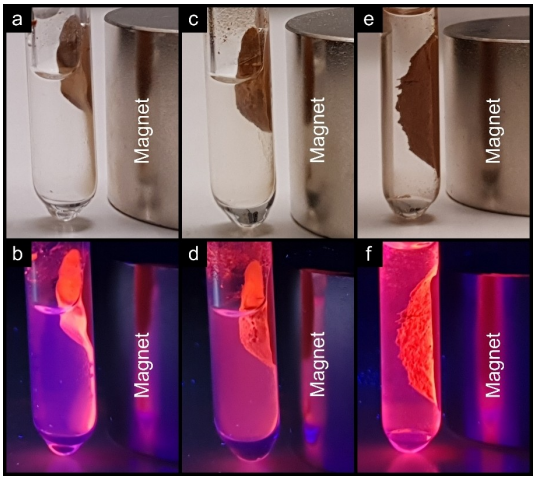

Figure 11. SPIONs@EuMOF-4 composites synthesized in water (a, b), ethanol (c, d), and cyclohexane (e, f) under visible (a, c, e) and UV light (λ_{exc} = 302 nm, b, d, f).

Figure S22) are observable. This shows that the formation of the inverse core-satellite structuring is independent of the selected solvent and that the composites are stable in different solvents.

Further Investigations on Property Dependencies

Additionally, investigations on the influence of the deprotonation grade of the citric acid stabilization were performed. No significant differences in magnetic and photophysical properties were observed when the stabilization pH value was adjusted to 4.0, 5.6 or 7.5 instead of 2.1. Accordingly, the formation of the inverse core-satellite composites is independent of the deprotonation grade of citric acid. Detailed information on the investigations are provided in the supporting information.

Conclusion

Strongly luminescent Ln-based metal-organic frameworks $^3_\infty[Ln_2(BDC)_3(H_2O)_4]$ (Ln=Eu, Tb; BDC^{2-} = terephthalate) were successfully combined with superparamagnetic, citrate-stabilized iron oxide nanoparticles (SPIONs) to composites according to an inverse core-satellite functionalization mode with core-satellite character. Within, luminescent MOF crystallites act as core material partly covered by magnetic satellite nanoparticles. The inverse functionalization mode allows for a finetuning of the inherent properties of both components, magnetism and luminescence, by means of magnetization and emission intensity. Such defined and quantitative steering of properties, especially of the luminescence intensity, is not achievable for the previously reported core-shell composites with a luminescent MOF as closed shell around a magnetic core. In the inverse concept, the MOF crystallites can be only partly coated with the iron oxide nanoparticles. As a result, the luminescence intensity is not only influenced by simple "dilution" of the luminescent MOF within the non-luminescent material but also by the light-absorbing nature of iron oxide itself. Thereby, the luminescence mechanisms themselves are not influenced by the magnetic satellite nanoparticle shell apart from light absorption, as proven by lifetime determinations. Thereby, the luminescence intensity becomes tuneable through the amount of magnetic material. In addition, also the colour of the emitted light can be tuned by selecting different ratios of different lanthanide MOFs, such as Eu/Tb–BDC–MOFs. The chromaticity can be mathematically corrected regarding the absorption of iron oxide nanoparticles leading to a quantitative approach towards chromaticity differences.

The saturation magnetization can be directly adjusted linearly by a defined weight ratio of the components, $^3_\infty[Ln_2(BDC)_3(H_2O)_4]$ (Ln=Tb, Eu) and citrate-stabilized Fe_3O_4 nanoparticles. Thereby, the selected component weight ratio corresponds to the weight ratio of the constituents in the composite.

Furthermore, the constituents are not separable by washing, ultrasonication and magnetic separation and can be synthesized in different solvents, indicating a remarkable stability of the synthesized composites.

In addition to the steering character of photophysical and magnetic properties, the new luminomagnetic inverse core-satellite SPIONs@MOF composites offer options for a utilization as luminescent, magnetic ink or anticounterfeiting protection. Thereby, the mutual dependence of saturation magnetization and luminescence intensity allows e.g. producing a forgery protection that has the characteristics of a specific ID with defined saturation magnetization and luminescence intensity. This could reach from a barely visible but instrumentally detectable photoluminescence of a specific colour combined with a high saturation magnetization to the direct opposite. Not only the structure and stability, but also the tunability of properties, which would not be achievable with core-shell particles imparting a magnetic core and a MOF shell, of the presented composites allows for multiple options of adjustment

to the respective needs beyond the previously reported MOF containing composites.

Experimental Section

Detailed information on the analytical methods is provided in the supporting information.

Materials: Europium(III) nitrate hexahydrate ($Eu(NO_3)_3 \cdot 6H_2O$, 99.9% (REO), abcr GmbH), terbium(III) nitrate hexahydrate ($Tb(NO_3)_3 \cdot 6H_2O$, 99.9% (REO), abcr GmbH), terephthalic acid ($C_8H_6O_4$, 98%, abcr GmbH), sodium hydroxide (NaOH, 98% (p.a.), Grüssing GmbH), Iron(II) chloride tetrahydrate ($FeCl_2 \cdot 4H_2O$, 99%, Sigma-Aldrich), iron(III) chloride hexahydrate ($FeCl_3 \cdot 6H_2O$, 99%, Sigma-Aldrich), citric acid monohydrate ($C_6H_8O_7 \cdot H_2O$, $\geq$99%, Sigma-Aldrich), ammonia solution ($NH_{3(aq)}$, 28–30%, Roth), and ethanol (C_2H_5OH, 97%, Stockmeier Chemie Gmbh & Co. KG) were used as purchased and without further purification.

Synthesis of citrate-stabilized Fe_3O_4 nanoparticles (SPIONs): Superparamagnetic iron oxide nanoparticles (SPIONs) were synthesized *via* the established method of co-precipitation.[44] 2.16 g (8.00 mmol) of $FeCl_3 \cdot 6H_2O$ and 795 mg (4.00 mmol) of $FeCl_2 \cdot 4H_2O$ were dissolved in deionized water (100 mL) and precipitated with 5 mL ammonia solution (28–30 wt%) under stirring. Afterwards the obtained precipitate was washed with water until reaching a neutral pH. Subsequently, for stabilization purposes, 100 mL of a 50 mM citric acid solution was added, whose pH was adjusted to 2.1, 4.0, 5.6, or 7.5 with aqueous ammonia solution. Afterwards, the obtained nanoparticles were washed several times to remove the excess of citric acid and finally vacuum dried at 70 °C. The obtained particles were investigated by TEM revealing an approximate size of 10 nm (see Figure S5). The hydrodynamic particle diameter of SPIONs was determined to 21 nm (±10 nm), 23 nm (±11 nm), 23 nm (±10 nm), and 24 nm (±11 nm) for SPIONs citrate-stabilized at 2.1, 4.0, 5.6, and 7.5 (Figure S29). Considering the formation of a solvent shell around the particles, this corresponds with the particle size by observed TEM. PXRD analysis evinces the particles containing iron oxide in the magnetite structure (see Figure S4 and Figure S25). IR spectra show characteristic bands of citrate and iron oxide and therefore confirm the nanoparticles composition comprising of iron oxide and citrate (see Figure S6 and Figure S26).

Synthesis of Na_2BDC: Disodium terephthalate (Na_2BDC) was synthesized according to the literature[45] with slight adaptions. Briefly, 4.98 g (30.0 mmol) of terephthalic acid (H_2BDC) and 3.59 g (90.0 mmol) of sodium hydroxide (NaOH) were mixed with 60 mL deionized water and heated under reflux and stirring for one hour resulting in a clear solution. Subsequently, 30 mL ethanol were added to the boiling solution leading to the formation of a white precipitate. The mixture was filtered hot over a sintered glass filter funnel and the obtained colourless solid was dried in vacuum. Phase purity was confirmed by NMR spectroscopy and elemental analysis. The yield was 42% based on terephthalic acid. 1H NMR (400 MHz, D_2O, δ): 4.79 (s, D_2O), 7.89 (s, H, Ar H); Anal. calcd. for $C_8H_4Na_2O_4$: C 45.75, H 1.92, N, 0.00; found: C 45.04; H 1.80; N 0.00.

Synthesis of $^3_\infty[Eu_2(BDC)_3(H_2O)_4]$: The synthesis of $^3_\infty[Eu_2(BDC)_3(H_2O)_4]$ (BDC = benzene-1,4-dicarboxylate) was performed in an adapted synthesis based on a synthesis procedure for $^3_\infty[Ln_2(BDC)_3(H_2O)_4]$ reported in the literature.[36] In a typical synthesis 892 mg (2.00 mmol) of europium nitrate hexahydrate ($Eu(NO_3)_3 \cdot 6H_2O$) and 840 mg (4.00 mmol) of previously synthesized disodium terephthalate (Na_2BDC) were separately dissolved in 10 mL deionized water, each. The solutions were combined and stirred overnight leading to the formation of a white precipitate. The solid was separated by filtration over a sintered glass filter funnel, washed thrice with 20 mL of deionized water each, and dried in vacuum. The identity and phase purity of $^3_\infty[Eu_2(BDC)_3(H_2O)_4]$ were confirmed by powder X-ray diffraction (see Figure S2) and elemental analysis. SEM investigations reveal a crystallite size of approximately 50–500 nm (see Figure 2) corresponding with the particle diameter of 255 nm (±170 nm) determined by dynamic light scattering (see Figure S3). The yield was 64% based on Eu. IR (KBr): ν = 3464 (br), 3066 (w), 1609 (m), 1587 (m), 1545 (s), 1506 (s), 1420 (s), 1407 (s), 1310 (m), 1163 (w), 1139 (w), 1099 (w), 1021 (w), 884 (w), 829 (w), 762 (m), 751 (m), 586 (m), 558 (m), 530 (m), 510 (m), 437 cm^{-1} (w). Anal. calcd. for $C_{24}H_{20}O_{16}Eu_2$: C 33.20, H 2.32, N 0.00; found: C 32.92, H 2.28, N, 0.00.

Synthesis of $^3_\infty[Tb_2(BDC)_3(H_2O)_4]$: The synthesis of $^3_\infty[Tb_2(BDC)_3(H_2O)_4]$ was performed analogously to $^3_\infty[Eu_2(BDC)_3(H_2O)_4]$in an adapted synthesis based on the procedure reported for $^3_\infty[Ln_2(BDC)_3(H_2O)_4]$[36] using $Tb(NO_3)_3 \cdot 6H_2O$ instead of $Eu(NO_3)_3 \cdot 6H_2O$. The identity and phase purity of $^3_\infty[Tb_2(BDC)_3(H_2O)_4]$ were confirmed by powder X-ray diffraction (see Figure S2) and elemental analysis. The yield was 90% based on Tb. Anal. calcd. for $C_{24}H_{20}O_{16}Tb_2$: C 32.67, H 2.28, N: 0.00; found: C 32.30, H 2.31, N 0.00.

Synthesis of the composites SPIONs@LnMOF-*x*: To prepare the composites SPIONs@LnMOF-*x* (Ln=Eu, Tb), the synthesized, citrate-stabilized iron oxide nanoparticles (SPIONs) and the luminescent MOF $^3_\infty[Eu_2(BDC)_3(H_2O)_4]$, or $^3_\infty[Tb_2(BDC)_3(H_2O)_4]$ were combined in defined MOF:SPIONs weight ratios. The luminescent compound(s) and iron oxide nanoparticles were finely grounded in an agate mortar for five minutes. The obtained homogeneous mixture was transferred into a Duran® glass ampoule and a solvent (water, cyclohexane, or ethanol) was added. The ratio of the solid components and the solvent was thereby adjusted to 1:16 (solid:solvent, e.g. for synthesis of SPIONs@EuMOF-4: 40 mg $^3_\infty[Eu_2(BDC)_3(H_2O)_4]$, 10 mg SPIONs, 0.8 mL water; For applied component masses and solvent amount see Table S5). The resulting mixture was degassed by freezing in liquid nitrogen, evacuating the ampoule and letting the mixture thaw again. This procedure was repeated once more. Afterwards, the mixture was frozen and the ampoule was evacuated and sealed. The reaction mixture then was homogenized in an ultrasonic bath for three minutes. The ampoule was shaken and placed in a corundum oven, which was heated up within five hours to a temperature approximately 10 °C above the boiling point of the used solvent (110 °C for water, 90 °C for ethanol and cyclohexane), held at this temperature for five hours, followed by cooling down to room temperature in five hours. After the synthesis, the ampoule was opened, the resulting luminomagnetic composite material was magnetically separated from the liquid phase, and subsequently dried in vacuum (0.001 mbar) for one hour. The composite character of the resulting products was confirmed by powder X-ray diffraction and SEM/EDX, as well as TEM investigations and stability tests. Additionally, the luminescence and magnetic properties were investigated.

Synthesis of the composite SPIONs@EuTbMOF-4: Citrate-stabilized superparamagnetic iron oxide nanoparticles (SPIONs), $^3_\infty[Eu_2(BDC)_3(H_2O)_4]$ (Eu–BDC) and $^3_\infty[Tb_2(BDC)_3(H_2O)_4]$ (Tb–BDC) in a Tb–BDC:Eu–BDC:SPIONs weight ratio of 2:2:1 were mixed in an agate mortar and solvothermally treated analogously to the described synthesis procedure of SPIONs@LnMOF-*x*. Applied amounts of the constituents are listed in Table S5.

Washing procedure for SPIONs@EuMOF-4 composites: Three samples of SPIONs@EuMOF-4 were separately synthesized according to the synthesis procedure described above. After solvother-

mal treatment, the resulting reaction mixtures were transferred into a 10 mL screw cap glass and filled to 5 mL each, followed by treating with ultrasound for five minutes. Subsequently, the screw cap vessels were placed beside a neodymium magnet for five minutes followed by a rotation by 180°. This step was repeated three times, followed by a magnetic separation of the composites for five minutes, again. The liquid phases were removed and 5 mL deionized water were added in each vessel. The whole washing procedure was repeated two, four, or seven times, followed by drying in vacuum, resulting in SPIONs@EuMOF-4 composites, which were washed three, five or eight times in whole with almost unchanged magnetization (see Figure 10).

Acknowledgements

The authors gratefully acknowledge funding of the German Research Foundation (DFG) within the project MU-1562/7-2 and MA-7252/4-2 (Formation and properties of opto-magnetic hybrid materials via the influence of external stimuli). Open Access funding enabled and organized by Projekt DEAL.

Conflict of Interest

The authors declare no conflict of interest.

Data Availability Statement

The data that support the findings of this study are available in the supplementary material of this article.

Keywords: composites · core-shell nanostructures · luminescence · magnetism · metal-organic frameworks

[1] A. Amini, M. Khajeh, A. R. Oveisi, S. Daliran, M. Ghaffari-Moghaddam, H. S. Delarami, *J. Ind. Eng. Chem.* **2021**, *93*, 322.
[2] S. Wang, Y. Zhang, Y. Li, K. Chen, Y. Dai, D. Zhou, A. Ali, S. Yang, X. Xu, T. Jiang et al., *Mater. Des.* **2021**, *205*, 109707.
[3] a) W. Zhang, S. Shan, J. Fan, F. Yuan, T. Lawson, L. Kong, R. Hu, Y. Liu, *Macromol. Biosci.* **2021**, e2100082; b) E. J. Bealer, K. Kavetsky, S. Dutko, S. Lofland, X. Hu, *Int. J. Mol. Sci.* **2019**, *21*, 186; c) M. Kalaj, M. S. Denny, K. C. Bentz, J. M. Palomba, S. M. Cohen, *Angew. Chem. Int. Ed.* **2019**, *58*, 2336; d) C.-W. Zhao, Y.-A. Li, X.-R. Wang, G.-J. Chen, Q.-K. Liu, J.-P. Ma, Y.-B. Dong, *Chem. Commun.* **2015**, *51*, 15906; e) L. Malfatti, P. Falcaro, B. Marmiroli, H. Amenitsch, M. Piccinini, A. Falqui, P. Innocenzi, *Nanoscale* **2011**, *3*, 3760; f) C. Dimitrakakis, B. Marmiroli, H. Amenitsch, L. Malfatti, P. Innocenzi, G. Grenci, L. Vaccari, A. J. Hill, B. P. Ladewig, M. R. Hill et al., *Chem. Commun.* **2012**, *48*, 7483; g) B. Tatykayev, F. Donat, H. Alem, L. Balan, G. Medjahdi, B. Uralbekov, R. Schneider, *ACS Omega* **2017**, *2*, 4946; h) P. Falcaro, R. Ricco, A. Yazdi, I. Imaz, S. Furukawa, D. Maspoch, R. Ameloot, J. D. Evans, C. J. Doonan, *Coord. Chem. Rev.* **2016**, *307*, 237.
[4] P. Lu, J.-L. Zhang, Y.-L. Liu, D.-H. Sun, G.-X. Liu, G.-Y. Hong, J.-Z. Ni, *Talanta* **2010**, *82*, 450.
[5] a) F. Ke, L. Wang, J. Zhu, *Nanoscale* **2015**, *7*, 1201; b) M. M. Mostafavi, F. Movahedi, *Appl. Organomet. Chem.* **2018**, *32*, e4217; c) Y. Wu, Y. Ma, G. Xu, F. Wei, Y. Ma, Q. Song, X. Wang, T. Tang, Y. Song, M. Shi et al., *Sens. Actuators B* **2017**, *249*, 195; d) C.-F. Zhang, L.-G. Qiu, F. Ke, Y.-J. Zhu, Y.-P. Yuan, G.-S. Xu, X. Jiang, *J. Mater. Chem. A* **2013**, *1*, 14329.
[6] W. Li, G. Li, D. Liu, *RSC Adv.* **2016**, *6*, 94113.
[7] a) F. Ke, L.-G. Qiu, J. Zhu, *Nanoscale* **2014**, *6*, 1596; b) L. Li, K. K. Sun, L. Fan, W. Hong, Z. S. Xu, L. Liu, *Mater. Lett.* **2014**, *126*, 197.
[8] a) Y. Chen, X. Huang, X. Feng, J. Li, Y. Huang, J. Zhao, Y. Guo, X. Dong, R. Han, P. Qi et al., *Chem. Commun.* **2014**, *50*, 8374; b) Y. Hu, S. Zheng, F. Zhang, *Front. Chem. Sci. Eng.* **2016**, *10*, 534; c) L. Wang, S. Yang, L. Chen, S. Yuan, Q. Chen, M.-Y. He, Z.-H. Zhang, *Catal. Sci. Technol.* **2017**, *7*, 2356.
[9] H.-X. Zhao, Q. Zou, S.-K. Sun, C. Yu, X. Zhang, R.-J. Li, Y.-Y. Fu, *Chem. Sci.* **2016**, *7*, 5294.
[10] S.-H. Huo, X.-P. Yan, *Analyst* **2012**, *137*, 3445.
[11] M. Aghayi-Anaraki, V. Safarifard, *Eur. J. Inorg. Chem.* **2020**, *2020*, 1916.
[12] R. Ricco, L. Malfatti, M. Takahashi, A. J. Hill, P. Falcaro, *J. Mater. Chem. A* **2013**, *1*, 13033.
[13] T. Zhang, X. Zhang, X. Yan, L. Kong, G. Zhang, H. Liu, J. Qiu, K. L. Yeung, *Chem. Eng. J.* **2013**, *228*, 398.
[14] A. Schejn, T. Mazet, V. Falk, L. Balan, L. Aranda, G. Medjahdi, R. Schneider, *Dalton Trans.* **2015**, *44*, 10136.
[15] Q. Yang, Q. Zhao, S. Ren, Q. Lu, X. Guo, Z. Chen, *J. Solid State Chem.* **2016**, *244*, 25.
[16] A. Pinna, R. Riccó, R. Migheli, G. Rocchitta, P. A. Serra, P. Falcaro, L. Malfatti, P. Innocenzi, *RSC Adv.* **2018**, *8*, 25664.
[17] F. Cheng, E. S. Marshall, A. J. Young, P. J. Robinson, J.-S. G. Bouillard, A. M. Adawi, N. A. Vermeulen, O. K. Farha, M. R. Reithofer, J. M. Chin, *Chem. Eur. J.* **2017**, *23*, 15578.
[18] a) S. Pal, D. Jagadeesan, K. L. Gurunatha, M. Eswaramoorthya, T. K. Maji, *J. Mater. Chem.* **2008**,*18*, 5448; b) T. Wehner, K. Mandel, M. Schneider, G. Sextl, K. Müller-Buschbaum, *ACS Appl. Mater. Interfaces* **2016**, *8*, 5445.
[19] T. Wehner, M. T. Seuffert, J. R. Sorg, M. Schneider, K. Mandel, G. Sextl, K. Müller-Buschbaum, *J. Mater. Chem. C* **2017**, *5*, 10133.
[20] M. T. Seuffert, S. Wintzheimer, M. Oppmann, T. Granath, J. Prieschl, A. Alrefai, H.-J. Holdt, K. Müller-Buschbaum, K. Mandel, *J. Mater. Chem. C* **2020**, *8*, 16010.
[21] B. C. Ma, S. Ghasimi, K. Landfester, F. Vilela, K. A. I. Zhang, *J. Mater. Chem. A* **2015**, *3*, 16064.
[22] Y. Sahoo, H. Pizem, T. Fried, D. Golodnitsky, L. Burstein, C. N. Sukenik, G. Markovich, *Langmuir* **2001**, *17*, 7907.
[23] a) K. S. Wilson, L. A. Harris, J. D. Goff, J. S. Riffle, J. P. Dailey, *Eur. Cells Mater.* **2002**, *3*, 206; b) J. S. Basuki, A. Jacquemin, L. Esser, Y. Li, C. Boyer, T. P. Davis, *Polym. Chem.* **2014**, *5*, 2611.
[24] S. Laurent, D. Forge, M. Port, A. Roch, C. Robic, L. Vander Elst, R. N. Muller, *Chem. Rev.* **2008**, *108*, 2064.
[25] Y. Sahoo, A. Goodarzi, M. T. Swihart, T. Y. Ohulchanskyy, N. Kaur, E. P. Furlani, P. N. Prasad, *J. Phys. Chem. B* **2005**, *109*, 3879.
[26] a) S.-M. Yu, A. Laromaine, A. Roig, *J. Nanopart. Res.* **2014**, *16*, 2484; b) M. A. Dheyab, A. A. Aziz, M. S. Jameel, O. A. Noqta, P. M. Khaniabadi, B. Mehrdel, *Sci. Rep.* **2020**, *10*, 10793; c) T. Granath, K. Mandel, P. Löbmann, *Part. Part. Syst. Charact.* **2022**, *39*, 2100279.
[27] a) C.-J. Yu, S.-M. Wu, W.-L. Tseng, *Anal. Chem.* **2013**, *85*, 8559; b) S. Nigam, K. C. Barick, D. Bahadur, *J. Magn. Magn. Mater.* **2011**, *323*, 237; c) A. Manciulea, A. Baker, J. R. Lead, *Chemosphere* **2009**, *76*, 1023.
[28] P. Yang, Z. Quan, Z. Hou, C. Li, X. Kang, Z. Cheng, J. Lin, *Biomaterials* **2009**, *30*, 4786.
[29] a) L. Huang, M. He, B. Chen, B. Hu, *J. Mater. Chem. A* **2015**, *3*, 11587; b) S. E. Moradi, A. M. Haji Shabani, S. Dadfarnia, S. Emami, *Anal. Methods* **2016**, *8*, 6337; c) Y. Wang, Y. Zhang, C. Hou, M. Liu, *RSC Adv.* **2015**, *5*, 98260.
[30] a) T. Wang, P. Zhao, N. Lu, H. Chen, C. Zhang, X. Hou, *Chem. Eng. J.* **2016**, *295*, 403; b) T. Wang, S. Liu, G. Gao, P. Zhao, N. Lu, X. Lun, X. Hou, *Microchim. Acta* **2017**, *184*, 2981.
[31] Y. Hu, Z. Huang, J. Liao, G. Li, *Anal. Chem.* **2013**, *85*, 6885.
[32] S. Balakrishnan, A. Launikonis, P. Osvath, G. F. Swiegers, A. P. Douvalis, G. J. Wilson, *Mater. Chem. Phys.* **2010**, *120*, 649.
[33] W. Mnasri, L. B. Tahar, P. Beaunier, D. A. Haidar, M. Boissière, O. Sandre, S. Ammar, *Nanomaterials* **2020**, *10*, 393.
[34] T. M. Reineke, M. Eddaoudi, M. Fehr, D. Kelley, O. M. Yaghi, *J. Am. Chem. Soc.* **1999**, *121*, 1651.
[35] a) J.-C. G. Bünzli, S. Comby, A.-S. Chauvin, C. D. Vandevyver, *J. Rare Earth* **2007**, *25*, 257; b) J.-C. G. Bünzli, C. Piguet, *Chem. Soc. Rev.* **2005**, *34*, 1048; c) K. Binnemans, *Chem. Rev.* **2009**, *109*, 4283.
[36] C. Daiguebonne, N. Kerbellec, O. Guillou, J.-C. Bünzli, F. Gumy, L. Catala, T. Mallah, N. Audebrand, Y. Gérault, K. Bernot et al., *Inorg. Chem.* **2008**, *47*, 3700.
[37] M. E. Fleet, *Acta Crystallogr., Sect. B: Struct. Crystallogr. Cryst. Chem.* **1981**, *37*, 917.
[38] W. T. Carnall, P. R. Fields, K. Rajnak, *J. Chem. Phys.* **1968**, *49*, 4450.
[39] I. Balberg, H. L. Pinch, *J. Magn. Magn. Mater.* **1978**, *7*, 12.

[40] I. Nimeroff, J. R. Rosenblatt, M. C. Dannemiller, *J. Res. Natl. Bur. Stand. Sect. A* **1961**, *65 A*, 475.
[41] V. Haquin, M. Etienne, C. Daiguebonne, S. Freslon, G. Calvez, K. Bernot, L. Le Pollès, S. E. Ashbrook, M. R. Mitchell, J.-C. Bünzli et al., *Eur. J. Inorg. Chem.* **2013**, *2013*, 3464.
[42] W. T. Carnall, P. R. Fields, K. Rajnak, *J. Chem. Phys.* **1968**, *49*, 4447.
[43] M. S. Wrighton, D. S. Ginley, D. L. Morse, *J. Phys. Chem.* **1974**, *78*, 2229.
[44] R. Massart, *IEEE Trans. Magn.* **1981**, *17*, 1247.
[45] J. Kaduk, *Acta Crystallogr., Sect. B: Struct. Sci., Cryst. Eng. Mater.* **2000**, *56*, 474.

Manuscript received: November 8, 2022
Revised manuscript received: December 6, 2022
Accepted manuscript online: December 7, 2022